Article

The Effect of Charge, Isospin, and Strangeness in the QCD Phase Diagram Critical End Point

Krishna Aryal [1], Constantinos Constantinou [2,3], Ricardo L. S. Farias [4] and Veronica Dexheimer [1,*]

[1] Department of Physics, Kent State University, Kent, OH 44242, USA; karyal@kent.edu
[2] INFN-TIFPA, Trento Institute of Fundamental Physics and Applications, 38123 Povo, TN, Italy; cconstantinou@ectstar.eu
[3] European Centre for Theoretical Studies in Nuclear Physics and Related Areas, 38123 Villazzano, TN, Italy
[4] Departamento de Física, Universidade Federal de Santa Maria, Santa Maria, RS 97105-900, Brazil; ricardo.farias@ufsm.br
[*] Correspondence: vdexheim@kent.edu

Abstract: In this work, we discuss the deconfinement phase transition to quark matter in hot/dense matter. We examine the effect that different charge fractions, isospin fractions, net strangeness, and chemical equilibrium with respect to leptons have on the position of the coexistence line between different phases. In particular, we investigate how different sets of conditions that describe matter in neutron stars and their mergers, or matter created in heavy-ion collisions affect the position of the critical end point, namely where the first-order phase transition becomes a crossover. We also present an introduction to the topic of critical points, including a review of recent advances concerning QCD critical points.

Keywords: phase transition; critical point; quark matter

1. Introduction to Critical Points

In thermodynamics, a critical point refers to the end point of a phase equilibrium curve. The presence of a critical point was first identified by Charles Cagniard de la Tour in 1822 [1]. He observed that, above a critical temperature, there was a continuous transition of elements in a gun barrel from liquid to vapour. A couple of decades later, Faraday (1845) studied the liquefying of gases, and Mendeleev (1860) [2] measured a vanishing point of liquid–vapour surface tension naming it "Absolute boiling temperature" [3]. Finally, in 1869, Andrews studied many different substances, establishing the continuity of vapour–liquid phases and creating the name and modern concept of "critical point" [4]. In theoretical research, van der Waals(1873) [5] contributed by providing an equation of state with a critical point for the liquid–gas transition. Smoluchowski [6] and Einstein [7] (1908, 1910) explained critical opalescence, the phenomenon by which a liquid at the critical point becomes opaque to a collimated beam of laser light, which results from fluctuations becoming comparable in size with the wavelength of light, and causing scattering. These led to Landau's classical theory of critical phenomena, Fisher, Kadanoff, and Wilson scaling, and, eventually, to a full fluctuation-based formulation of renormalization group theory [8].

The question arises whether there exists a critical point associated with the phase expected to be found at high-energy density, namely chirally symmetric matter composed of deconfined quarks and gluons, similar to the critical point of liquid-vapour transitions. Quantum Chromodynamics describes the fundamental constituents of matter, quarks and gluons,

as being almost massless, however, hadrons are massive. The mass of hadrons, which is associated with the breaking of chiral symmetry, is the source of most visible mass in the universe. The constituents of QCD carry color charge and experience the strong force, although they are normally confined within the hadrons. High-energy collisions deconfine those charges, producing the quark-gluon plasma. Finding the QCD critical point experimentally in heavy-ion experiments is a formidable task currently being pursued at the Relativistic Heavy Ion Collider (RHIC) [9,10]. Additional studies will be possible when dedicated facilities enter into operation, such as Nuclotron-based Ion Collider fAcility (NICA) [11] and Facility for Antiproton and Ion Research (FAIR) [12].

At zero baryon chemical potential, $\mu_B = 0$, baryons and antibaryons or quarks and antiquarks are in chemical equilibrium (with respect to the strong, not the weak force) with one another. In this case, at finite temperature, it is possible to determine the QCD pressure and additional thermodynamic quantities numerically with controllable accuracy on the lattice. Calculations at finite quark masses, in which case the chiral symmetry of QCD is not exact, do not exhibit the presence of a critical point (at $\mu_B = 0$). However, notable changes in properties of matter with increasing temperature appear. The significant rise in pressure with increasing temperature indicates the change in phase from a hadron gas to a quark-gluon plasma. However, this transition is not sharp. In other words, there is no point at which those phases coexist, despite one phase continuously transforming into another, which is referred to as a crossover [13].

The approximate location of a critical point when $\mu_B \neq 0$, may be found through extrapolations performed by calculating coefficients of a Taylor expansion around $\mu_B = 0$ and using assumptions from analyticity and convergence [14,15]. Complementary approaches using holographic gauge/gravity correspondence to map the fluctuations of baryon charge in the dense quark-gluon liquid onto a numerically tractable gravitational problem involving the charge fluctuations of holographic black holes have been able to predict the position of the QCD critical point at $T = 89$ MeV , $\mu_B = 724$ MeV [16]. For other theoretical models that also predict the existence and position of the QCD critical point see References [17–19].

Alternatively to μ_B, QCD phase diagrams are also studied in the temperature-isospin chemical potential, μ_I, plane. The later is advantageous due to the fact that lattice QCD results are not afflicted by the sign problem at finite μ_I, as long as $\mu_B = 0$. When $\mu_B \neq 0$ or, equivalently, when there is a difference in the number of particles and anti-particles in the system, the first-principle methods such as non-perturbative lattice QCD simulations cannot be implemented [20–22]. Finite μ_I, zero μ_B calculations have recently received a lot of attention due to their relevance to heavy-ion collisions [23], compact stars [24–26] and even to the evolution of the early Universe [27]. These calculations can be used to verify if the predictions of effective models of QCD are reliable when compared with first principle calculations [28–34]. In the case of QCD at finite isospin density, the first lattice simulations of References [35,36] were performed using unphysical pion masses and/or unphysical flavor content. The results from these first simulations were in qualitative agreement with the different approaches to QCD [37–70]. More recently, lattice QCD results for finite isospin density were implemented using an improved lattice action with staggered fermions at physical quark and pion masses [71–74], their predictions being in very good agreement with the results obtained from updated chiral perturbation theory [75–77] and Nambu–Jona-Lasinio (NJL) models [78–81].

For $\mu_B = 0$, in the regime of small temperatures and small μ_I, the system is said to be composed of so-called normal matter, NM, without pion condensation. Increasing only the temperature, the system enters a phase in which chiral symmetry is partially restored and quarks are deconfined, that is the expected quark-gluon plasma phase. On the other hand, for low temperature and increasing μ_I, the system reaches the onset of the pion condensation, PC,

phase through a second-order phase transition. The PC onset takes place at $\mu_I = m_\pi$. For $\mu_I < m_\pi$ there is a smooth crossover related to the chiral symmetry restoration and deconfinement transitions, and the pion condensate vanishes for all temperatures. For $\mu_I > m_\pi$, one can find a critical temperature at which there is a second order phase transition from the PC to the QGP phase. In this case, there is a lattice QCD prediction for a pseudo-triple point, where the NM, quark-gluon plasma, and PC phases meet [71,74]. There are also other calculations, such as a recent work using the non-local Polyakov-loop-extended Nambu–Jona–Lasinio (PNJL) model [82], which is in excellent agreement with lattice QCD calculations for the QCD phase diagram at finite μ_I.

In this work, we combine both approaches discussed above and study three-dimensional QCD phase diagrams as a function of temperature, baryon chemical potential, and either charge fraction, Y_Q, or isospin fraction, Y_I. The relation among the two charges is trivial only when net strangeness is zero. A fixed fraction is achieved by self-consistently determining the respective (charge or isospin) chemical potential. In this work, we consider two particular cases, one in which strangeness is constrained to be zero (same amount of strange and anti-strange particles, achieved by self-consistently determining the respective strange chemical potential, μ_S), and one in which strangeness is free to vary (in which case $\mu_S = 0$). We focus, in particular, on how the end point of the first-order phase transition line changes for particular cases associated with different astrophysical and laboratory scenarios.

2. Our Formalism

In order to study the effects of different conditions on the critical point, we first describe the formalism that allows us to reproduce a deconfinement first-order phase transition that eventually (at large temperatures) becomes a crossover. This phase transition is necessarily tied to a chiral-symmetry restoration phase transition (independently of the transition order), as they are connected through the effective masses of hadrons and quarks, in which the respective order parameters for both kinds of phase transition appear (see Equations (67) in Reference [83]). It is very important to note that such a formalism must contain the degrees of freedom expected to be found on both sides of the coexistence line in order to fully determine how conditions such as strangeness affect these degrees of freedom and, ultimately, moves the coexistence line and critical end point to a different part of the QCD phase diagram. We satisfy this requirement by making use of the Chiral Mean Field (CMF) model which is an effective relativistic mean-field model that describes baryons, quarks, and leptons within the same formalism [83]. It is based on a non-linear realization of the sigma model [84] within the mean-field approximation.

The model has been shown to give a good description of the dense matter inside proto-neutron and neutron stars [85,86]. This includes reproducing i) 2 solar masses neutron stars, or even more massive ones when higher-order vector interactions are used [86], ii) radii that agree with The Laser Interferometer Gravitational-Wave Observatory (LIGO) results [87] provided throught the use of spectral equation of state, or both methods (throught the use of spectral equation of state and universal relations [88,89]) when vector isovector couplings are included (all 90% confidence) [90], and iii) The Neutron star Interior Composition Explorer (NICER) results for radii (90% confidence) [91–94]. We have also analyzed the differences that arise from the relaxation of the assumption of local conserved quantities, such as electric charge and lepton fraction, to global quantities (the latter for the first time) [95]. We found that, although such relaxation widens the phase transition as a function of baryon chemical potential or free energy (less for the fixed lepton fraction case), there is no change in the position of the critical point. This is a result of the dominance of thermal effects around the deconfinement critical point which is not the case for the nuclear liquid–gas phase transition, as discussed in detail in Reference [96]. Since in this work we focus on the discussion of

critical points, we assume that the surface tension of quark matter is very large (of the order of hundreds of MeV), in which case mixtures of phases do not appear and ours constraints related to strangeness, charge, and isospin can be carried out locally. More complicated cases will be studied in the future.

At low densities, the model was fit to nuclear saturation properties at zero temperature and lattice QCD data at large temperatures. The latter includes a first order phase transition at $T = 270$ MeV and a pressure functional P(T) similar to References [97,98] at vanishing baryon chemical potential for pure gauge, a crossover at vanishing baryon chemical potential with a transition temperature of 171 MeV (determined as the peak of the change of the chiral condensate and the parameter for deconfinement), and the location of the critical endpoint (at $\mu_{B_{cr}} = 354$ MeV, $T_{cr} = 167$ MeV for symmetric matter) in accordance with Reference [99]. In the past, this formalism was used to simulate particle multiplicities, rapidity distributions, and flow in heavy-ion collisions [100] and the differences among stellar matter vs. matter produced in heavy-ion collisions in the vicinity of the deconfinement coexistence line, drawing analogies with the nuclear liquid–gas phase diagram [96]. More recently, we used this formalism to construct three-dimensional QCD phase diagrams up to a temperature $T = 160$ MeV, the other two axes being the chemical potential (μ_B or $\tilde{\mu}$), and either the charge or isospin fractions [101]. In this work, we go further by extending coexistence lines all the way to the respective critical end points and discussing the effects of different conditions on the relative position of the critical end points. In the following, we summarize the different situations under consideration. We begin by defining a few relevant quantities.

The free energy per baryon under fixed charge and strangeness is defined as [102]

$$\tilde{\mu} = \mu_B + Y_Q \mu_Q + Y_S \mu_S \,, \tag{1}$$

where μ_Q, μ_I, and μ_S are the charge, isospin, and strange chemical potentials, respectively. Alternatively, under fixed isospin and strangeness [101]

$$\widetilde{\mu} = \mu'_B + Y_I \mu_I + Y_S \mu'_S, \tag{2}$$

where, under the new constraints, the chemical potentials transform as $\mu_I = \mu_Q$, $\mu'_B = \mu_B + \frac{1}{2}\mu_Q$, and $\mu'_S = \mu_S - \frac{1}{2}\mu_Q$. These definitions reproduce the same equilibrium equations described in Appendix A of Reference [101], independently of the chosen constraints. The free energy per baryon $\tilde{\mu}$ is the quantity which is the same in both phases in the case of a first-order phase transition (both sides of the coexistence line). The charge fraction, $Y_Q = \frac{Q}{B}$, isospin fraction, $Y_I = \frac{I}{B}$, and strangeness fraction, $Y_S = \frac{S}{B}$, are defined as the baryonic (hadrons + quarks) electric charge, isospin, and strangeness over the total baryon number. The relation between charge and isospin fractions depends on the strangeness following Reference [101] is

$$Y_I = Y_Q - \frac{1}{2} + \frac{1}{2}Y_S \,. \tag{3}$$

3. Results

The different conditions we discuss in this work relate to systems created in very short-lived heavy-ion collisions, where there is no sufficient time for significant net strangeness to be produced, $Y_S = 0$, and astrophysical conditions, where net strangeness is expected to be produced, $Y_S \neq 0$. While matter generated in heavy-ion collisions and supernova explosions is close to being isospin symmetric, matter in neutron stars and their mergers [103] is far from that, possessing very low charge fraction. Some simple cases that approximate these conditions are:

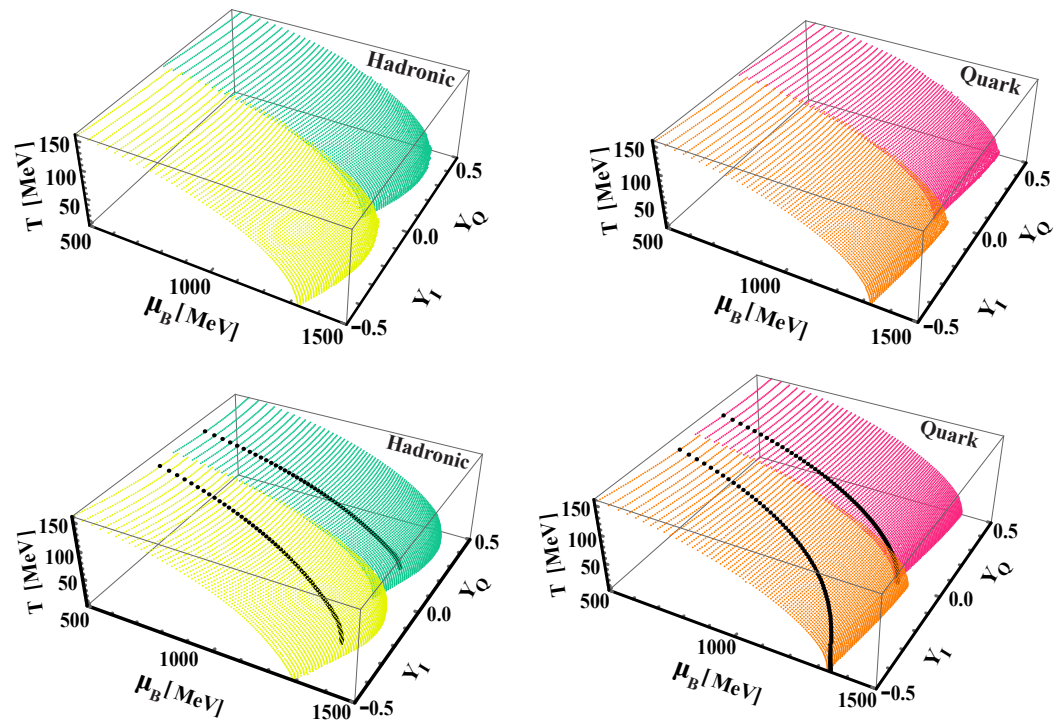- $Y_Q = 0$ and $Y_S = 0$ (equivalent to $Y_I = -0.5$ and $Y_S = 0$) ;

- $Y_Q = 0.5$ and $Y_S = 0$ (equivalent to $Y_I = 0$ and $Y_S = 0$) ;
- $Y_Q = 0$ and $Y_S \neq 0$;
- $Y_I = -0.5$ and $Y_S \neq 0$;
- $Y_Q = 0.5$ and $Y_S \neq 0$;
- $Y_I = 0$ and $Y_S \neq 0$;
- $Y_Q = -Y_{\text{lepton}}$ and $Y_S \neq 0$,

where in the last case electrons and muons were introduced in chemical equilibrium with the baryons and quarks, $\mu_e = \mu_\mu = -\mu_Q$. Note that, despite first appearances, conditions 3-4 and 5-6 are *not* equivalent. As already mentioned in Section 1, this is because the relation between Y_I and Y_Q is a trivial shift only when net strangeness is zero, but not otherwise. See Reference [104] for a complete discussion of the chemically equilibrated case at finite temperature.

Figure 1 shows three-dimensional deconfinement first-order phase-transition regions calculated finding a discontinuity in the order parameter for deconfinement. The left panels show values for the baryon chemical potential μ_B on the hadronic side, while the right panels show values for μ_B on the quark side of the coexistence region. Their difference stems from the fact that we are plotting them as a function of baryon chemical potential (not free energy per baryon) and that μ_Q or μ_I is different in each phase. The different colors show calculations performed by varying the charge fraction from $0 \to 0.5$ (shown as a function of Y_Q) and the isospin fraction from $-0.5 \to 0$ (shown as a function of Y_I). The top panels were calculated fixing the net strangeness to zero and, as a consequence, are a perfect 0.5 shift in the fraction axis (see Equation (3)). The bottom panels had no strangeness constraint and, therefore, present a finite net strangeness. As a result, the two pairs of surfaces are not only shifted but also *deformed* relative to one another. This leads to more pronounced differences (from the top panels) at large temperatures, where strangeness is abundant. The bottom panels also show a chemically equilibrated line which, at low temperatures, follows a much lower value of charge or isospin fraction in the quark phase.

At the largest temperature we show in Figure 1, 160 MeV, it is easy to see that the phases are very similar, but no further analysis was made to find the exact position of the critical end point. In some cases, our region went into the crossover phase, marking the steepest change in order parameters (peak of susceptibility) instead of the position of the first-order phase transition. The critical end point occurs when the pressure (grand-potential density) as a function of the deconfinement order parameter, exhibits a single maximum (minimum) instead of two. For a more focused exploration of the exact position of our critical end point, we present in Figure 2 two-dimensional phase diagrams for deconfinement for the five of the seven cases described in the previous section. These are the cases in which the free energy per baryon equals the baryon chemical potential. From Equation (1) it is quite obvious that this happens for $Y_Q = 0$. It also happens when $Y_I = 0$, meaning that $\mu_Q = 0$. This is the case no matter if the strangeness is being constrained or not. In the chemical equilibrium case, the total charge ($Y_Q + Y_{\text{lepton}}$) is zero, implying once more $\tilde{\mu} = \mu_B$, but we only investigate this for the case with net strangeness, as this is the case associated with chemically-equilibrated stars.

Analyzing Figure 2 in more detail, one can see that both lower charge or isospin fraction and the constraint of zero net strangeness weaken the phase transition, shifting the critical end point to a lower temperature (and, as a consequence, to a larger μ_B). When combined, these features cause the green curve to shrink and the green dot to be found more than 21 MeV below the beige inverted triangle, which represents the "opposite" case ($Y_I = 0$ and $Y_S \neq 0$). A lower critical temperature means that the first order transition between the phases becomes weaker faster with the increase of temperature compared to the other cases. This can be seen in the size of the discontinuity in energy density or other derivatives of the grand potential across the transition and it is related to how different or similar the two phases are.
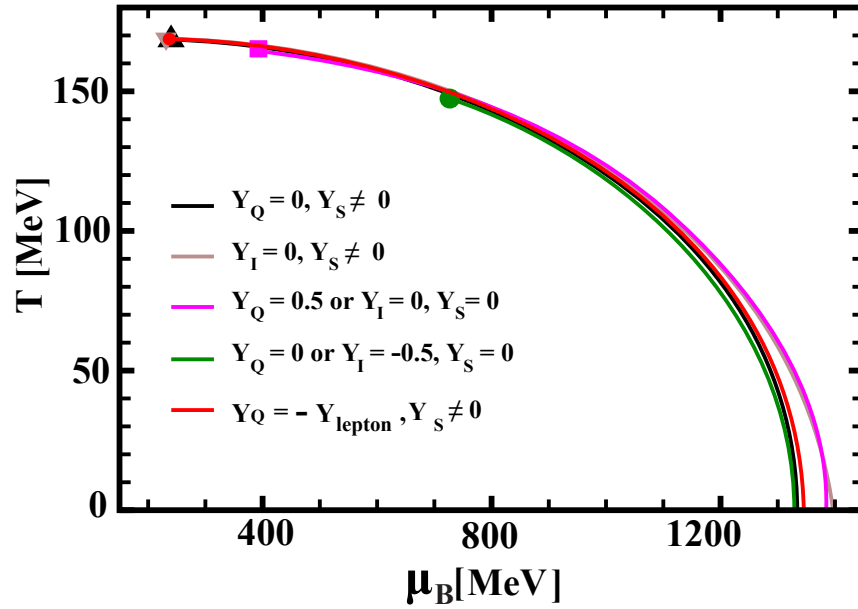
Figure 1. lThree-dimensional QCD phase diagrams showing temperature, baryon chemical potential, and either charge fraction (dark green/pink regions) or isospin fraction (light green/orange regions regions). The left panels show the hadronic side of the coexistence line, while the right panels show the quark side. The top panels show matter with zero net strangeness ($Y_S = 0$), while the bottom panels show matter with net strangeness ($Y_S \neq 0$). The black lines on the bottom panels show charge neutral, strange matter in chemical equilibrium with leptons.
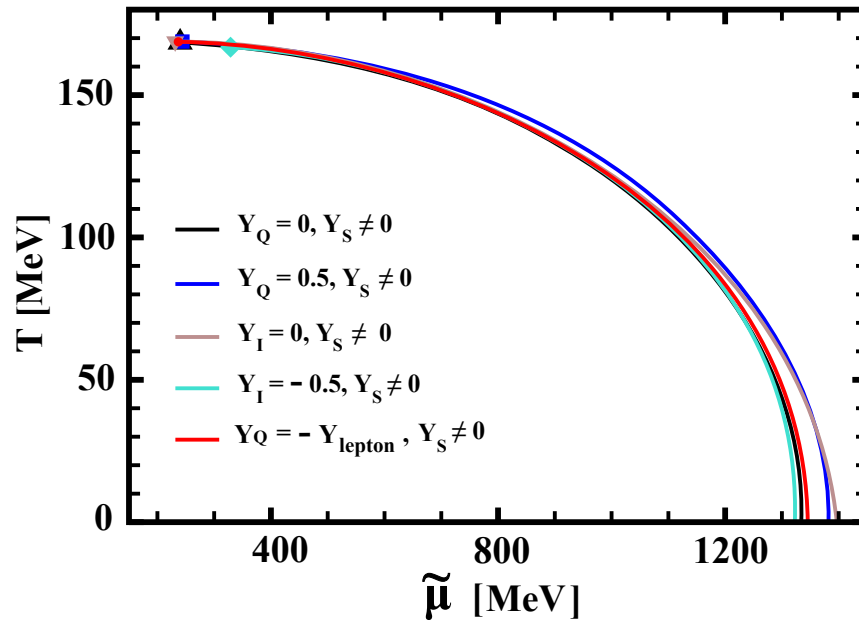
The coexistence line for the chemically-equilibrated case is clearly more similar to the $Y_Q = 0$ cases at low temperatures (when μ_Q is more negative, see Figure 2 of [105]), and becomes slowly more similar to the $Y_S \neq 0$ at large temperatures, when strangeness is abundant.

Numerical values for the critical end point and for the $T = 0$ portion of the phase diagram are given in Table 1. For some of the cases, the baryon chemical potential is different in each phase which, again, traces back to Equation (3). The cases in which this happens, namely $Y_Q = 0.5$ and $Y_I = -0.5$ in the presence of net strangeness, are shown in Figure 3, together with the other cases with strangeness for comparison. Here the critical end point is only distinguishable for the $Y_I = -0.5$ case, in which the critical temperature is a bit lower and the free energy per baryon larger than the other cases. It was shown in Reference [106], using the NJL and the PNJL models to study instabilities in quark matter related to the liquid–gas phase transition, that large isospin asymmetries (more negative Y_I) and net strangeness weaken the first-order phase transition, making it easier for it to become a crossover. This is in partial agreement with what we found in this work (we found the opposite with respect to strangeness). This difference is related to the fact that in our case the critical end point is strongly affected by the presence of hadrons.

Concerning the general position of the lines in Figure 3, as discussed in detail in Reference [101] for the specific case of zero and large temperatures, larger charge fractions or smaller isospin fractions (both meaning more balanced amount of protons and neutrons or up and down quarks when not considering strangeness) push the phase transition to larger

Figure 2. Temperature versus baryon chemical potential for several cases with different fixed charge or isospin fractions with and without net strangeness, plus the particular case of chemical equilibrium with leptons. In all cases the baryon chemical potential equals the free energy per baryon.

Figure 3. Temperature versus free energy per baryon for several cases with different fixed charge or isospin fractions but always with net strangeness, plus the particular case of chemical equilibrium with leptons. Strangeness is not constrained.

baryon chemical potentials at a given temperature. This has to do with how much more this change softens hadronic matter, so the quark phase becomes more energetically favored at lower energy densities, which corresponds to larger baryon chemical potentials. The coex-

Table 1. Summary of baryon chemical potential, free energy per baryon, and temperature at the critical end point and the baryon chemical potential (in either side of the coexistence line) and free energy per baryon at zero temperature under differing conditions of strangeness, fixed charge/isospin fraction or in chemical equilibrium with leptons. All units are in MeV.

Cases	$\mu_{B_{cr}}$	$\tilde{\mu}_{cr}$	T_{cr}	$\mu_{B_0}^Q$	$\mu_{B_0}^H$	$\tilde{\mu}_0$
$Y_Q = 0, Y_s \neq 0$	240.1	240.1	168.5	1334.0	1333.0	1334.0
$Y_I = 0, Y_s \neq 0$	231.4	231.4	168.8	1396.7	1396.8	1396.7
$Y_Q = 0.5, Y_s = 0$	392.7	392.7	165.2	1382.0	1381.0	1382.0
$Y_Q = 0, Y_s = 0$	727.1	727.1	147.4	1329.0	1328.0	1329.0
$Y_Q = 0.5, Y_s \neq 0$	227.6	244.0	168.8	1382.0	1381.0	1382.0
$Y_I = -0.5, Y_s \neq 0$	295.9	328.9	166.8	1322.8	1314.3	1322.8
$Y_Q = -Y_{\text{lep}}, Y_s \neq 0$	236.9	236.9	168.7	1345.5	1345.4	1345.5

istence line for the chemically-equilibrated case is clearly more similar to the $Y_Q = 0$ and $Y_I = -0.5$ cases at low temperatures.

4. Conclusions

After an introduction to the topic of critical points, we discussed qualitative results for critical end points reproduced by the CMF model. In order to do so, we first built three-dimensional phase diagrams showing the deconfinement coexistence region as a function of temperature, baryon chemical potential, and either charge fraction ,Y_Q, or isospin fraction, Y_I. We also analyzed different scenarios concerning zero or unconstrained net strangeness fraction, Y_S, and presented results for the particular case of weak chemical equilibrium with leptons.

We then focused on different specific cases for combinations of $Y_Q = 0$, $Y_Q = 0.5$, $Y_I = 0$, $Y_I = -0.5$, weak chemical equilibrium, $Y_S = 0$, and $Y_S \neq 0$. The isospin symmetric and the large charge fraction cases present a later (in both baryon chemical potential and free energy per baryon) phase transition at low temperatures. These cases correspond to matter created in heavy-ion collisions or in supernova explosions. At large temperatures, all curves are close, but some extend to significantly lower baryon chemical potentials and free energies. The ones that do not, and therefore present a distinguished critical end point, are the non-strange cases, once more corresponding to matter created in heavy-ion collisions. This feature had not been investigated before within the CMF model.

For astrophysical conditions, corresponding to larger net strangeness content and negative isospin fraction (or low charge fraction), this means an earlier confinement phase transition (lower value of baryon chemical potential and free energy per baryon) and a still strong transition that extends high in temperature. This is an encouraging result, as it has been shown that strong first-order phase transitions can leave distinguishable signals in the post merger part of gravitational wave signals from neutron star mergers [107].

Informed Consent Statement: text.

Data Availability Statement: text.

Conflicts of Interest: The authors declare no conflict of interest.

List of Acronyms

- **CMF** Chiral Mean Field
- **FAIR** Facility for Antiproton and Ion Research
- **LIGO** Laser Interferometer Gravitational-Wave Observatory
- **NICA** Nuclotron-based Ion Collider fAcility
- **NICER** Neutron star Interior Composition Explorer
- **NJL** Nambu–Jona-Lasinio
- **NM** Normal matter
- **PC** Pion condensation
- **PNJL** Polyakov-loop-extended Nambu–Jona–Lasinio
- **QCD** Quantum Chromodynamics
- **QGP** Quark–gluon plasma
- **RHIC** Relativistic Heavy Ion Collider

References

1. Arago, F.; Gay-Lussac, J. *Annales de chimie et de physique*; Chez Crochard, 1822.
2. Mendeleev, D. Chastichnoe stseplenie nekotoruikh zhidkikh organicheskikh soedinienii. *Khimicheskii zhurnal N. Sokolova i A. Engel'garta* **1860**, *3*, 81–97.
3. Faraday, M. On the Liquefaction and Solidification of Bodies Generally Existing as Gases. Abstracts of the Papers Communicated to the Royal Society of London. *JSTOR* **1843**, *5*, 540–542.
4. Andrews, T. XVIII. The Bakerian Lecture.—On the continuity of the gaseous and liquid states of matter. *Philos. Trans. R. Soc. Lond.* **1869**, 575–590.
5. Van der Waals, J.D. *Over de Continuiteit van den Gas-en Vloeistoftoestand*; Sijthoff: Amsterdam, The Netherlands, 1873; Volume 1.
6. v. Smoluchowski, M. Molekular-kinetische Theorie der Opaleszenz von Gasen im kritischen Zustande, sowie einiger verwandter Erscheinungen. *Annalen der Physik* **1908**, *330*, 205–226.
7. Einstein, A. Theorie der Opaleszenz von homogenen Flüssigkeiten und Flüssigkeitsgemischen in der Nähe des kritischen Zustandes. *Annalen der Physik* **1910**, *338*, 1275–1298.
8. Stephanov, M.A.; Rajagopal, K.; Shuryak, E.V. Signatures of the tricritical point in QCD. *Phys. Rev. Lett.* **1998**, *81*, 4816–4819, doi:10.1103/PhysRevLett.81.4816.
9. Bzdak, A.; Esumi, S.; Koch, V.; Liao, J.; Stephanov, M.; Xu, N. Mapping the Phases of Quantum Chromodynamics with Beam Energy Scan. *Phys. Rept.* **2020**, *853*, 1–87, doi:10.1016/j.physrep.2020.01.005.
10. An, X.; Bluhm, M.; Du, L.; Dunne, G.V.; Elfner, H.; Gale, C.; Grefa, J.; Heinz, U.; Huang, A.; Karthein, J.M.; et al. The BEST framework for the search for the QCD critical point and the chiral magnetic effect. *Nucl. Phys. A* **2022**, *1017*, 122343
11. Senger, P. The heavy-ion program of the future FAIR facility. *J. Phys. Conf. Ser.* **2017**, *798*, 012062. doi:10.1088/1742-6596/798/1/012062.
12. Kekelidze, V.; Kovalenko, A.; Lednicky, R.; Matveev, V.; Meshkov, I.; Sorin, A.; Trubnikov, G. Feasibility study of heavy-ion collision physics at NICA JINR. *Nucl. Phys. A* **2017**, *967*, 884–887. doi:10.1016/j.nuclphysa.2017.06.031.
13. Aoki, Y.; Endrodi, G.; Fodor, Z.; Katz, S.D.; Szabo, K.K. The Order of the quantum chromodynamics transition predicted by the standard model of particle physics. *Nature* **2006**, *443*, 675–678, doi:10.1038/nature05120.
14. Gavai, R.V.; Gupta, S. The Critical end point of QCD. *Phys. Rev. D* **2005**, *71*, 114014, doi:10.1103/PhysRevD.71.114014.
15. Fodor, Z.; Giordano, M.; Günther, J.N.; Kapás, K.; Katz, S.D.; Pásztor, A.; Portillo, I.; Ratti, C.; Sexty, D.; Szabó, K.K. Trying to constrain the location of the QCD critical endpoint with lattice simulations. *Nucl. Phys. A* **2019**, *982*, 843–846, doi:10.1016/j.nuclphysa.2018.12.015.
16. Critelli, R.; Noronha, J.; Noronha-Hostler, J.; Portillo, I.; Ratti, C.; Rougemont, R. Critical point in the phase diagram of primordial quark-gluon matter from black hole physics. *Phys. Rev. D* **2017**, *96*, 096026, doi:10.1103/PhysRevD.96.096026.
17. Halasz, A.M.; Jackson, A.D.; Shrock, R.E.; Stephanov, M.A.; Verbaarschot, J.J.M. On the phase diagram of QCD. *Phys. Rev. D* **1998**, *58*, 096007, doi:10.1103/PhysRevD.58.096007.

18. Stephanov, M.A. QCD phase diagram and the critical point. *Prog. Theor. Phys. Suppl.* **2004**, *153*, 139–156, doi:10.1142/S0217751X05027965.

19. Ayala, A.; Zamora, B.A.; Cobos-Martínez, J.J.; Hernández-Ortiz, S.; Hernández, L.A.; Raya, A.; Tejeda-Yeomans, M.E. Collision energy dependence of the critical end point from baryon number fluctuations in the Linear Sigma Model with quarks. *arXiv* **2021**, arXiv:2108.02362.

20. Karsch, F. Lattice QCD at high temperature and density. *Lect. Notes Phys.* **2002**, *583*, 209–249, doi:10.1007/3-540-45792-5_6.

21. Muroya, S.; Nakamura, A.; Nonaka, C.; Takaishi, T. Lattice QCD at finite density: An Introductory review. *Prog. Theor. Phys.* **2003**, *110*, 615–668, doi:10.1143/PTP.110.615.

22. Bedaque, P.F. A complex path around the sign problem. *EPJ Web Conf.* **2018**, *175*, 01020, doi:10.1051/epjconf/201817501020.

23. Li, B.A.; Ko, C.M.; Bauer, W. Isospin physics in heavy ion collisions at intermediate-energies. *Int. J. Mod. Phys. E* **1998**, *7*, 147–230, doi:10.1142/S0218301398000087.

24. Migdal, A.B.; Saperstein, E.E.; Troitsky, M.A.; Voskresensky, D.N. Pion degrees of freedom in nuclear matter. *Phys. Rept.* **1990**, *192*, 179–437. doi:10.1016/0370-1573(90)90132-L.

25. Steiner, A.W.; Prakash, M.; Lattimer, J.M.; Ellis, P.J. Isospin asymmetry in nuclei and neutron stars. *Phys. Rept.* **2005**, *411*, 325–375, doi:10.1016/j.physrep.2005.02.004.

26. Brandt, B.B.; Endrodi, G.; Fraga, E.S.; Hippert, M.; Schaffner-Bielich, J.; Schmalzbauer, S. New class of compact stars: Pion stars. *Phys. Rev. D* **2018**, *98*, 094510, doi:10.1103/PhysRevD.98.094510.

27. Schwarz, D.J.; Stuke, M. Lepton asymmetry and the cosmic QCD transition. *JCAP* **2009**, *11*, 025, [Erratum: JCAP 10, E01 (2010)], doi:10.1088/1475-7516/2009/11/025.

28. Cotter, S.; Giudice, P.; Hands, S.; Skullerud, J.I. Towards the phase diagram of dense two-color matter. *Phys. Rev.* **2013**, *D87*, 034507, doi:10.1103/PhysRevD.87.034507.

29. Braguta, V.V.; Ilgenfritz, E.M.; Kotov, A.Yu.; Molochkov, A.V.; Nikolaev, A.A. Study of the phase diagram of dense two-color QCD within lattice simulation. *Phys. Rev.* **2016**, *D94*, 114510, doi:10.1103/PhysRevD.94.114510.

30. Bali, G.S.; Bruckmann, F.; Endrodi, G.; Fodor, Z.; Katz, S.D.; Schafer, A. QCD quark condensate in external magnetic fields. *Phys. Rev.* **2012**, *D86*, 071502, doi:10.1103/PhysRevD.86.071502.

31. Bali, G.S.; Bruckmann, F.; Endrodi, G.; Fodor, Z.; Katz, S.D.; Krieg, S.; Schafer, A.; Szabo, K.K. The QCD phase diagram for external magnetic fields. *JHEP* **2012**, *02*, 044, doi:10.1007/JHEP02(2012)044.

32. Bali, G.S.; Bruckmann, F.; Endrodi, G.; Katz, S.D.; Schafer, A. The QCD equation of state in background magnetic fields. *JHEP* **2014**, *08*, 177, doi:10.1007/JHEP08(2014)177.

33. Braguta, V.V.; Goy, V.A.; Ilgenfritz, E.M.; Kotov, A.Yu.; Molochkov, A.V.; Muller-Preussker, M.; Petersson, B. Two-Color QCD with Non-zero Chiral Chemical Potential. *JHEP* **2015**, *06*, 094, doi:10.1007/JHEP06(2015)094.

34. Braguta, V.V.; Ilgenfritz, E.M.; Kotov, A.Yu.; Petersson, B.; Skinderev, S.A. Study of QCD Phase Diagram with Non-Zero Chiral Chemical Potential. *Phys. Rev.* **2016**, *D93*, 034509, doi:10.1103/PhysRevD.93.034509.

35. Kogut, J.B.; Sinclair, D.K. Lattice QCD at finite isospin density at zero and finite temperature. *Phys. Rev. D* **2002**, *66*, 034505, doi:10.1103/PhysRevD.66.034505.

36. Kogut, J.B.; Sinclair, D.K. Quenched lattice QCD at finite isospin density and related theories. *Phys. Rev. D* **2002**, *66*, 014508, doi:10.1103/PhysRevD.66.014508.

37. Son, D.T.; Stephanov, M.A. QCD at finite isospin density. *Phys. Rev. Lett.* **2001**, *86*, 592–595, doi:10.1103/PhysRevLett.86.592.

38. Son, D.T.; Stephanov, M.A. QCD at finite isospin density: From pion to quark - anti-quark condensation. *Phys. Atom. Nucl.* **2001**, *64*, 834–842, doi:10.1134/1.1378872.

39. Lepori, L.; Mannarelli, M. Multicomponent meson superfluids in chiral perturbation theory. *Phys. Rev. D* **2019**, *99*, 096011, doi:10.1103/PhysRevD.99.096011.

40. Carignano, S.; Lepori, L.; Mammarella, A.; Mannarelli, M.; Pagliaroli, G. Scrutinizing the pion condensed phase. *Eur. Phys. J.* **2017**, *A53*, 35, doi:10.1140/epja/i2017-12221-x.

41. Janssen, O.; Kieburg, M.; Splittorff, K.; Verbaarschot, J.J.M.; Zafeiropoulos, S. Phase Diagram of Dynamical Twisted Mass Wilson Fermions at Finite Isospin Chemical Potential. *Phys. Rev. D* **2016**, *93*, 094502, doi:10.1103/PhysRevD.93.094502.

42. Cohen, T.D.; Sen, S. Deconfinement Transition at High Isospin Chemical Potential and Low Temperature. *Nucl. Phys.* **2015**, *A942*, 39–53, doi:10.1016/j.nuclphysa.2015.07.018.

43. Fraga, E.S.; Palhares, L.F.; Villavicencio, C. Quark mass and isospin dependence of the deconfining critical temperature. *Phys. Rev. D* **2009**, *79*, 014021, doi:10.1103/PhysRevD.79.014021.

44. Loewe, M.; Villavicencio, C. Thermal pions at finite isospin chemical potential. *Phys. Rev. D* **2003**, *67*, 074034, doi:10.1103/PhysRevD.67.074034.

45. Loewe, M.; Villavicencio, C. Two-flavor condensates in chiral dynamics: Temperature and isospin density effects. *Phys. Rev. D* **2005**, *71*, 094001, doi:10.1103/PhysRevD.71.094001.

46. Splittorff, K.; Son, D.T.; Stephanov, M.A. QCD - like theories at finite baryon and isospin density. *Phys. Rev. D* **2001**, *64*, 016003, doi:10.1103/PhysRevD.64.016003.

47. Mannarelli, M. Meson condensation. *Particles* **2019**, *2*, 411–443, doi:10.3390/particles2030025.

48. Khunjua, T.G.; Klimenko, K.G.; Zhokhov, R.N.; Zhukovsky, V.C. Inhomogeneous charged pion condensation in chiral asymmetric dense quark matter in the framework of NJL$_2$ model. *Phys. Rev. D* **2017**, *95*, 105010, doi:10.1103/PhysRevD.95.105010.

49. Khunjua, T.G.; Klimenko, K.G.; Zhokhov, R.N. Dualities in dense quark matter with isospin, chiral, and chiral isospin imbalance in the framework of the large-N$_c$ limit of the NJL$_4$ model. *Phys. Rev. D* **2018**, *98*, 054030, doi:10.1103/PhysRevD.98.054030.

50. Khunjua, T.G.; Klimenko, K.G.; Zhokhov, R.N. Chiral imbalanced hot and dense quark matter: NJL analysis at the physical point and comparison with lattice QCD. *Eur. Phys. J.* **2019**, *C79*, 151, doi:10.1140/epjc/s10052-019-6654-2.

51. Xia, T.; He, L.; Zhuang, P. Three-flavor Nambu–Jona-Lasinio model at finite isospin chemical potential. *Phys. Rev. D* **2013**, *88*, 056013, doi:10.1103/PhysRevD.88.056013.

52. Mu, C.f.; He, L.y.; Liu, Y.x. Evaluating the phase diagram at finite isospin and baryon chemical potentials in the Nambu–Jona-Lasinio model. *Phys. Rev. D* **2010**, *82*, 056006. doi:10.1103/PhysRevD.82.056006.

53. Abuki, H.; Anglani, R.; Gatto, R.; Pellicoro, M.; Ruggieri, M. The Fate of pion condensation in quark matter: From the chiral to the real world. *Phys. Rev. D* **2009**, *79*, 034032, doi:10.1103/PhysRevD.79.034032.

54. Andersen, J.O.; Kyllingstad, L. Pion Condensation in a two-flavor NJL model: the role of charge neutrality. *J. Phys. G* **2009**, *37*, 015003, doi:10.1088/0954-3899/37/1/015003.

55. Sun, G.f.; He, L.; Zhuang, P. BEC-BCS crossover in the Nambu-Jona-Lasinio model of QCD. *Phys. Rev. D* **2007**, *75*, 096004, doi:10.1103/PhysRevD.75.096004.

56. Ebert, D.; Klimenko, K.G. Pion condensation in electrically neutral cold matter with finite baryon density. *Eur. Phys. J.* **2006**, *C46*, 771–776, doi:10.1140/epjc/s2006-02527-5.

57. Ebert, D.; Klimenko, K.G. Gapless pion condensation in quark matter with finite baryon density. *J. Phys. G* **2006**, *32*, 599–608, doi:10.1088/0954-3899/32/5/001.

58. He, L.; Jin, M.; Zhuang, P. Pion Condensation in Baryonic Matter: from Sarma Phase to Larkin-Ovchinnikov-Fudde-Ferrell Phase. *Phys. Rev. D* **2006**, *74*, 036005, doi:10.1103/PhysRevD.74.036005.

59. He, L.y.; Jin, M.; Zhuang, P.f. Pion superfluidity and meson properties at finite isospin density. *Phys. Rev. D* **2005**, *71*, 116001, doi:10.1103/PhysRevD.71.116001.

60. He, L.; Zhuang, P. Phase structure of Nambu-Jona-Lasinio model at finite isospin density. *Phys. Lett.* **2005**, *B615*, 93–101, doi:10.1016/j.physletb.2005.03.066.

61. Barducci, A.; Casalbuoni, R.; Pettini, G.; Ravagli, L. A Calculation of the QCD phase diagram at finite temperature, and baryon and isospin chemical potentials. *Phys. Rev. D* **2004**, *69*, 096004, doi:10.1103/PhysRevD.69.096004.

62. Toublan, D.; Kogut, J.B. Isospin chemical potential and the QCD phase diagram at nonzero temperature and baryon chemical potential. *Phys. Lett.* **2003**, *B564*, 212–216, doi:10.1016/S0370-2693(03)00701-9.

63. Frank, M.; Buballa, M.; Oertel, M. Flavor mixing effects on the QCD phase diagram at nonvanishing isospin chemical potential: One or two phase transitions? *Phys. Lett.* **2003**, *B562*, 221–226, doi:10.1016/S0370-2693(03)00607-5.

64. Mukherjee, S.; Mustafa, M.G.; Ray, R. Thermodynamics of the PNJL model with nonzero baryon and isospin chemical potentials. *Phys. Rev. D* **2007**, *75*, 094015, doi:10.1103/PhysRevD.75.094015.

65. Bhattacharyya, A.; Ghosh, S.K.; Lahiri, A.; Majumder, S.; Raha, S.; Ray, R. Isospin symmetry breaking and baryon-isospin correlations from Polyakov−Nambu−Jona-Lasinio model. *Phys. Rev. C* **2014**, *89*, 064905, doi:10.1103/PhysRevC.89.064905.

66. Andersen, J.O.; Haque, N.; Mustafa, M.G.; Strickland, M. Three-loop hard-thermal-loop perturbation theory thermodynamics at finite temperature and finite baryonic and isospin chemical potential. *Phys. Rev.* **2016**, *D93*, 054045, doi:10.1103/PhysRevD.93.054045.

67. Adhikari, P.; Andersen, J.O.; Kneschke, P. Pion condensation and phase diagram in the Polyakov-loop quark-meson model. *Phys. Rev. D* **2018**, *98*, 074016, doi:10.1103/PhysRevD.98.074016.

68. Stiele, R.; Fraga, E.S.; Schaffner-Bielich, J. Thermodynamics of (2+1)-flavor strongly interacting matter at nonzero isospin. *Phys. Lett.* **2014**, *B729*, 72–78, doi:10.1016/j.physletb.2013.12.053.

69. Ueda, H.; Nakano, T.Z.; Ohnishi, A.; Ruggieri, M.; Sumiyoshi, K. QCD phase diagram at finite baryon and isospin chemical potentials in Polyakov loop extended quark meson model with vector interaction. *Phys. Rev. D* **2013**, *88*, 074006, doi:10.1103/PhysRevD.88.074006.

70. Kamikado, K.; Strodthoff, N.; von Smekal, L.; Wambach, J. Fluctuations in the quark-meson model for QCD with isospin chemical potential. *Phys. Lett.* **2013**, *B718*, 1044–1053, doi:10.1016/j.physletb.2012.11.055.

71. Brandt, B.B.; Endrodi, G.; Schmalzbauer, S. QCD phase diagram for nonzero isospin-asymmetry. *Phys. Rev. D* **2018**, *97*, 054514, doi:10.1103/PhysRevD.97.054514.

72. Brandt, B.B.; Endrodi, G.; Schmalzbauer, S. QCD at finite isospin chemical potential. *EPJ Web Conf.* **2018**, *175*, 07020, doi:10.1051/epjconf/201817507020.

73. Brandt, B.B.; Endrodi, G. QCD phase diagram with isospin chemical potential. *PoS* **2016**, *LATTICE2016*, 039, doi:10.22323/1.256.0039.

74. Brandt, B.B.; Endrodi, G.; Schmalzbauer, S. QCD at nonzero isospin asymmetry. *PoS* **2018**, *Confinement2018*, 260, doi:10.22323/1.336.0260.

75. Adhikari, P.; Andersen, J.O. QCD at finite isospin density: chiral perturbation theory confronts lattice data. *Phys. Lett.* **2020**, *B804*, 135352, doi:10.1016/j.physletb.2020.135352.

76. Adhikari, P.; Andersen, J.O. Pion and kaon condensation at zero temperature in three-flavor χPPT at nonzero isospin and strange chemical potentials at next-to-leading order. *JHEP* **2020**, *06*, 170, doi:10.1007/JHEP06(2020)170.

77. Adhikari, P.; Andersen, J.O.; Kneschke, P. Two-flavor chiral perturbation theory at nonzero isospin: Pion condensation at zero temperature. *Eur. Phys. J.* **2019**, *C79*, 874, doi:10.1140/epjc/s10052-019-7381-4.

78. Avancini, S.S.; Bandyopadhyay, A.; Duarte, D.C.; Farias, R.L.S. Cold QCD at finite isospin density: confronting effective models with recent lattice data. *Phys. Rev.* **2019**, *D100*, 116002, doi:10.1103/PhysRevD.100.116002.

79. Lopes, B.S.; Avancini, S.S.; Bandyopadhyay, A.; Duarte, D.C.; Farias, R.L.S. Hot QCD at finite isospin density: Confronting the SU(3) Nambu–Jona-Lasinio model with recent lattice data. *Phys. Rev. D* **2021**, *103*, 076023, doi:10.1103/PhysRevD.103.076023.

80. Lu, Z.Y.; Xia, C.J.; Ruggieri, M. Thermodynamics and susceptibilities of isospin imbalanced QCD matter. *Eur. Phys. J.* **2020**, *C80*, 46, doi:10.1140/epjc/s10052-020-7614-6.

81. Wu, Z.Q.; Ping, J.L.; Zong, H.S. QCD phase diagram at finite isospin and baryon chemical potentials with the self-consistent mean field approximation. *Chin. Phys. C* **2021**, *45*, 064102, doi:10.1088/1674-1137/abefc3.

82. Carlomagno, J.P.; Dumm, D.G.; Scoccola, N.N. Isospin asymmetric matter in a nonlocal chiral quark model. *arXiv* **2021**, arXiv:2107.02022.

83. Dexheimer, V.A.; Schramm, S. A Novel Approach to Model Hybrid Stars. *Phys. Rev. C* **2010**, *81*, 045201, doi:10.1103/PhysRevC.81.045201.

84. Papazoglou, P.; Zschiesche, D.; Schramm, S.; Schaffner-Bielich, J.; Stoecker, H.; Greiner, W. Nuclei in a chiral SU(3) model. *Phys. Rev. C* **1999**, *59*, 411–427, doi:10.1103/PhysRevC.59.411.

85. Roark, J.; Du, X.; Constantinou, C.; Dexheimer, V.; Steiner, A.W.; Stone, J.R. Hyperons and quarks in proto-neutron stars. *Mon. Not. Roy. Astron. Soc.* **2019**, *486*, 5441–5447, doi:10.1093/mnras/stz1240.

86. Dexheimer, V.; Gomes, R.O.; Klähn, T.; Han, S.; Salinas, M. GW190814 as a massive rapidly rotating neutron star with exotic degrees of freedom. *Phys. Rev. C* **2021**, *103*, 025808, doi:10.1103/PhysRevC.103.025808.

87. Abbott, B.P.; others. GW170817: Measurements of neutron star radii and equation of state. *Phys. Rev. Lett.* **2018**, *121*, 161101, doi:10.1103/PhysRevLett.121.161101.

88. Yagi, K.; Yunes, N. Binary Love Relations. *Class. Quant. Grav.* **2016**, *33*, 13LT01, doi:10.1088/0264-9381/33/13/13LT01.

89. Yagi, K.; Yunes, N. Approximate Universal Relations among Tidal Parameters for Neutron Star Binaries. *Class. Quant. Grav.* **2017**, *34*, 015006, doi:10.1088/1361-6382/34/1/015006.

90. Dexheimer, V.; de Oliveira Gomes, R.; Schramm, S.; Pais, H. What do we learn about vector interactions from GW170817? *J. Phys. G* **2019**, *46*, 034002, doi:10.1088/1361-6471/ab01f0.

91. Riley, T.E.; others. A *NICER* View of PSR J0030+0451: Millisecond Pulsar Parameter Estimation. *Astrophys. J. Lett.* **2019**, *887*, L21, doi:10.3847/2041-8213/ab481c.

92. Miller, M.C.; others. PSR J0030+0451 Mass and Radius from *NICER* Data and Implications for the Properties of Neutron Star Matter. *Astrophys. J. Lett.* **2019**, *887*, L24, doi:10.3847/2041-8213/ab50c5.

93. Riley, T.E.; others. A NICER View of the Massive Pulsar PSR J0740+6620 Informed by Radio Timing and XMM-Newton Spectroscopy. *Astrophys. J. Lett.* **2021**, *918*, L27, doi:10.3847/2041-8213/ac0a81.

94. Miller, M.C.; others. The Radius of PSR J0740+6620 from NICER and XMM-Newton Data. *Astrophys. J. Lett.* **2021**, *918*, L28, doi:10.3847/2041-8213/ac089b.

95. Roark, J.; Dexheimer, V. Deconfinement phase transition in proto-neutron-star matter. *Phys. Rev. C* **2018**, *98*, 055805, doi:10.1103/PhysRevC.98.055805.

96. Hempel, M.; Dexheimer, V.; Schramm, S.; Iosilevskiy, I. Noncongruence of the nuclear liquid–gas and deconfinement phase transitions. *Phys. Rev. C* **2013**, *88*, 014906, doi:10.1103/PhysRevC.88.014906.

97. Roessner, S.; Ratti, C.; Weise, W. Polyakov loop, diquarks and the two-flavour phase diagram. *Phys. Rev. D* **2007**, *75*, 034007, doi:10.1103/PhysRevD.75.034007.

98. Ratti, C.; Thaler, M.A.; Weise, W. Phases of QCD: Lattice thermodynamics and a field theoretical model. *Phys. Rev. D* **2006**, *73*, 014019, doi:10.1103/PhysRevD.73.014019.

99. Fodor, Z.; Katz, S.D. Critical point of QCD at finite T and mu, lattice results for physical quark masses. *JHEP* **2004**, *04*, 050, doi:10.1088/1126-6708/2004/04/050.

100. Steinheimer, J.; Dexheimer, V.; Petersen, H.; Bleicher, M.; Schramm, S.; Stoecker, H. Hydrodynamics with a chiral hadronic equation of state including quark degrees of freedom. *Phys. Rev. C* **2010**, *81*, 044913, doi:10.1103/PhysRevC.81.044913.

101. Aryal, K.; Constantinou, C.; Farias, R.L.S.; Dexheimer, V. High-Energy Phase Diagrams with Charge and Isospin Axes under Heavy-Ion Collision and Stellar Conditions. *Phys. Rev. D* **2020**, *102*, 076016, doi:10.1103/PhysRevD.102.076016.

102. Hempel, M.; Pagliara, G.; Schaffner-Bielich, J. Conditions for phase equilibrium in supernovae, protoneutron, and neutron stars. *Phys. Rev. D* **2009**, *80*, 125014. doi:10.1103/PhysRevD.80.125014.

103. Most, E.R.; Jens Papenfort, L.; Dexheimer, V.; Hanauske, M.; Stoecker, H.; Rezzolla, L. On the deconfinement phase transition in neutron-star mergers. *Eur. Phys. J. A* **2020**, *56*, 59, doi:10.1140/epja/s10050-020-00073-4.
104. Alford, M.G.; Haber, A.; Harris, S.P.; Zhang, Z. Beta equilibrium under neutron star merger conditions, 2021,
105. Dexheimer, V.; Aryal, K.; Wolf, .M.; Constantinou, .C.; Farias, R.L.S. Deconfinement Phase Transition under Chemical Equilibrium. *Astron. Nachr.* **2021**, *342*, 347–351, doi:10.1002/asna.202113932.
106. Liu, L.M.; Zhou, W.H.; Xu, J.; Peng, G.X. Isospin effect on quark matter instabilities. *Phys. Lett. B* **2021**, *822*, 136694.
107. Most, E.R.; Papenfort, L.J.; Dexheimer, V.; Hanauske, M.; Schramm, S.; Stöcker, H.; Rezzolla, L. Signatures of quark-hadron phase transitions in general-relativistic neutron-star mergers. *Phys. Rev. Lett.* **2019**, *122*, 061101, doi:10.1103/PhysRevLett.122.061101.